Mesh generation and computational modeling techniques for bioimpedance measurements: an example using the VHP data

2012 J. Phys.: Conf. Ser. 407 012004

(http://iopscience.iop.org/1742-6596/407/1/012004)

Journal of Physics: Conference Series **407** (2012) 012004 doi:10.1088/1742-6596/407/1/012004

Mesh generation and computational modeling techniques for bioimpedance measurements: an example using the VHP data

A A Danilov[1], V Yu Salamatova[2], Yu V Vassilevski[1]

[1]Institute of Numerical Mathematics, Russian Academy of Sciences
[2]Scientific-Educational Centre of the Institute of Numerical Mathematics, Russian Academy of Sciences

Email: a.a.danilov@gmail.com

Abstract. Here, a workflow for high-resolution efficient numerical modeling of bioimpedance measurements is suggested that includes 3D image segmentation, adaptive mesh generation, finite-element discretization, and the analysis of simulation results. Using the adaptive unstructured tetrahedral meshes enables to decrease significantly a number of mesh elements while keeping model accuracy. The numerical results illustrate current, potential, and sensitivity field distributions for a conventional Kubicek-like scheme of bioimpedance measurements using segmented geometric model of human torso based on Visible Human Project data. The whole body VHP man computational mesh is constructed that contains 574 thousand vertices and 3.3 million tetrahedrons.

1. Introduction

At present, computerized models of real human anatomy are widely used in various research areas such as radiography, nuclear medicine, radiation protection and other [1, 2]. The same is applied to impedance simulation studies (see, e.g., [3, 4]). Modeling of sensitivity distributions for various measurement schemes requires solving a number of well-defined computational problems using high-resolution anatomically accurate 3D models. Our aim was to describe mesh generation and computational modeling techniques for bioimpedance measurements based on high-resolution anatomical models of the human body. Using finite-element models on tetrahedral meshes, unlike conventional finite-difference schemes on cubic meshes, allows taking into account tissue anisotropy thus providing more realistic description of electric properties of the human body.

2. Segmentation and mesh generation

The original 3D image of the human torso was derived from the Visible Human Project data as a stack of 843 567×305 color images with resolution 1×1×1 mm [5]. We started from a partially segmented data of a human torso from the Voxel-Man project [6]. These data were primarily aimed at visualization purposes and contained a significant amount of unclassified tissue. From a computational point of view, void spaces between tissues were not allowed in a segmented model. So, a further processing of the segmented data was undertaken.

Most of the segmentation process was performed manually using ITK-SNAP segmentation software program [7]. In some cases semi-automatic threshold-based approach was used for specific tissues like fat, bones and blood vessels. At the final stage we used semi-automatic post-processing

algorithms for filling remaining gaps between tissues and final segmented data smoothing. These algorithms are based on mathematical morphology operations: erosion, dilation, opening and closing, connected-component labeling and Gaussian smoothing. Final steps are performed using Convert3D tool from ITK-SNAP package.

The geometrical model obtained from the image segmentation was used to create an unstructured tetrahedral mesh. For this, several approaches can be used, including marching cubes algorithm for surface reconstruction [8], surface triangulation smoothing and coarsening [9], 3D Delaunay triangulation, and advancing front technique for volume mesh generation [10]. Of these, we used the Delaunay triangulation algorithm from CGAL-Mesh library [11]. This algorithm permits defining a specific mesh size for each tissue and organ. So, we used a small mesh size for blood vessels and other organs and tissues with the similar geometrical features. A large mesh size was prescribed for gross tissues like fat or muscles. This approach allowed us to create computational meshes with a reasonably small number of elements still preserving the local geometric features of the segmented model.

The segmented model containing 26 labels describing major organs and tissues of the human torso and the generated mesh with 413.508 vertices and 2.315.329 tetrahedrons are shown in Fig. 1. This mesh represents most anatomical features of the human torso.

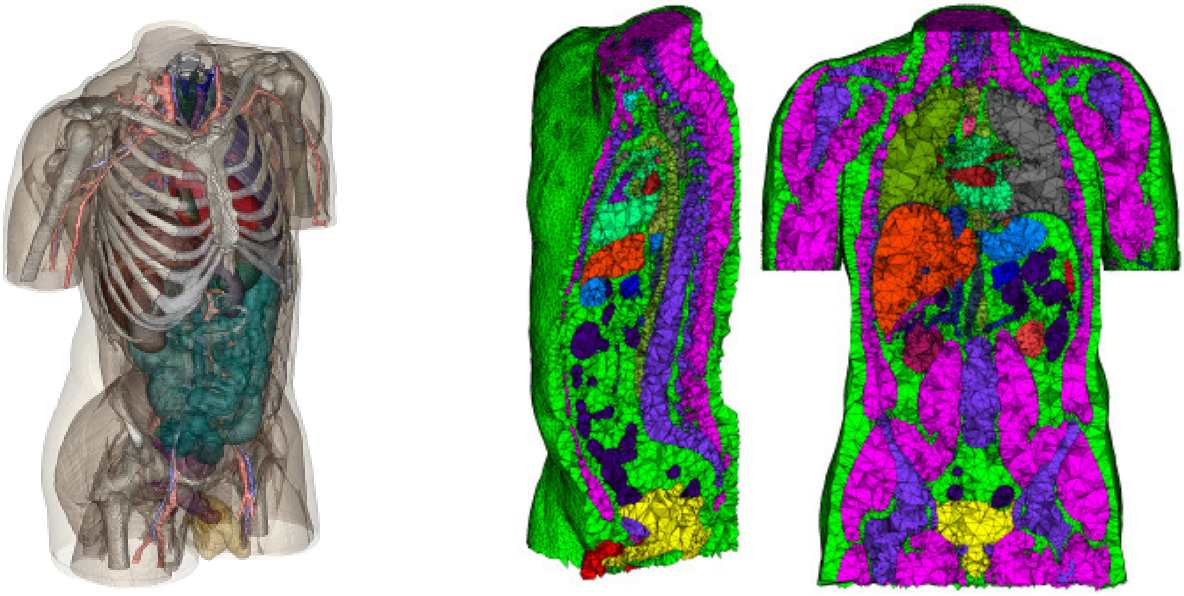

Fig. 1. Geometrical model of the segmented image (left) and unstructured tetrahedral meshes (right)

After mesh generation, we added a skin layer and multilayered electrodes to the surface of the constructed mesh. Boundary triangulation was used to create a prismatic mesh on the surface, and then each prism was split into three tetrahedrons resulting in a conformal mesh. Mesh cosmetics algorithms from the Ani3D library [12] were used to improve mesh quality. This essential step reduces discretization errors and condition number of the resulted systems of linear equations.

3. Mathematical model

The electrical fields generated during bioimpedance measurements are governed by the equation

$$\mathrm{div}(\mathbf{C}\nabla U) = 0 \quad \text{in } \Omega \qquad (1)$$

with the boundary conditions

$$(\mathbf{J},\mathbf{n}) = I_0 / S_{\pm} \quad \text{on } \Gamma_{\pm} \qquad (2)$$

$$(\mathbf{J},\mathbf{n}) = 0 \quad \text{on } \partial\Omega \backslash \Gamma_{\pm} \qquad (3)$$

$$U(x_0, y_0, z_0) = 0 \qquad (4)$$

$$\mathbf{J} = \mathbf{C}\nabla U \qquad (5)$$

where Ω – the computational domain, $\partial\Omega$ – its boundary, $\Gamma_{\pm}$ – electrode contact surfaces, $\mathbf{n}$ – external unit normal vector, U – electric potential, $\mathbf{C}$ – conductivity tensor, $\mathbf{J}$ – current density, I_0 – electric current, $S_{\pm}$ – area of the electrode contacts. Equation (1) determines the distribution of electric field in the domain with heterogeneous conductivity $\mathbf{C}$. Equation (2) sets a constant current density on the electrode contact surfaces. Equation (3) defines the no-flow condition on the boundary. Uniqueness of the solution is guaranteed by equation (4), where (x_0,y_0,z_0) – some point of the domain Ω.

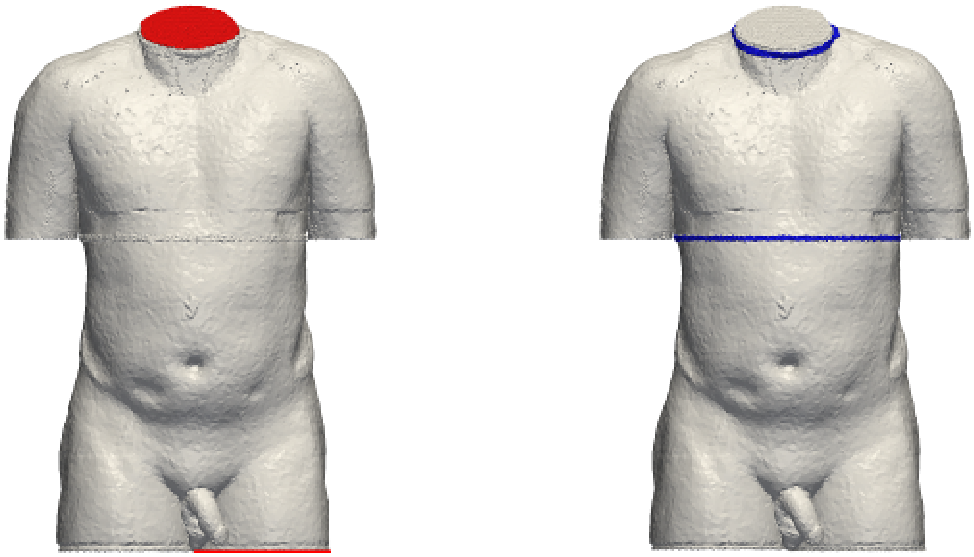

Fig. 2. Electrode configuration for Kubicek-like measurement scheme: current electrodes in red, voltage electrodes in blue

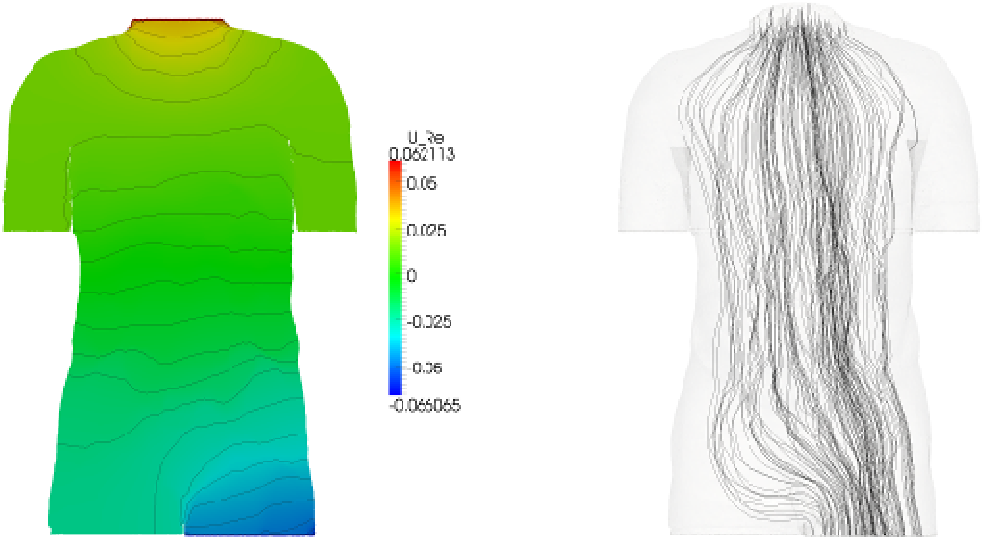

Fig. 3. Cutplane of the potential field and the respective current lines. Measurement frequency 50 kHz

Discretization of the equations (1)–(5) was obtained using finite element scheme with piecewise linear elements P1 on unstructured tetrahedral meshes. The resulting system of linear equations was solved by GMRES method with second-order ILU preconditioner [13]. Several numerical experiments were performed on simplified geometrical models for a convergence study of the proposed scheme.

These tests demonstrated first-order convergence on a series of unmatched meshes and nearly second order convergence on a series of nested meshes (data not shown).

4. Numerical results

Let us consider the Kubicek-like electrode configuration scheme [14] with a pair of current electrodes on the head and the left leg, and a pair of band voltage electrodes as depicted in Fig. 2. Since our calculations were performed on a torso segmented model, we applied the boundary conditions at the appropriate interfaces.

Fig. 4. Areas of high sensitivity, threshold 50% (left) and 70% (right). Measurement frequency 5 kHz

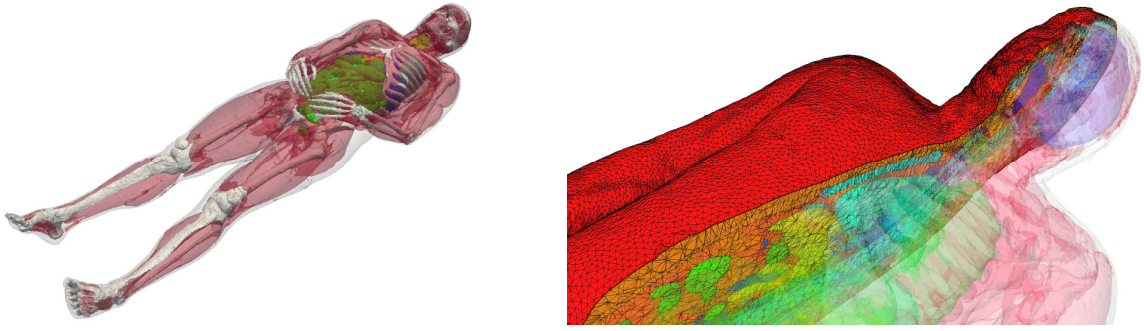

a *b*

Fig. 5. Segmented whole body model of the Visible Human Man (a) and a part of related generated mesh (b)

We defined the conductivity parameters for labeled tissues as in [15]. The simulations were performed for current frequencies 5 and 50 kHz. The computed current and potential field distributions are shown in Fig. 3. The results of sensitivity analysis are presented in Fig. 4 and Table 1 show good quantitative agreement with that of sensitivity distribution analysis made by Kauppinen et al. [3].

We used the proposed techniques to construct the computational mesh for the whole body model based on VHP data. The related segmented model containing 32 materials and generated mesh containing 574.128 vertices and 3.300.481 tetrahedrons are shown in Fig. 5.

Table 1. Relative contribution (%) of organs and tissues to the impedance signal

Organ/tissue	Measurement frequency		Organ/tissue	Measurement frequency	
	5 kHz	50 kHz		5 kHz	50 kHz
Muscles	72.56	69.44	Heart	0.64	1.01
Left lung	5.23	5.49	Bones	0.57	0.51
Right lung	4.59	5.03	Pancreas	0.47	0.45
Diaphragm	2.57	2.39	Liver	0.28	0.50
Oesophagus	2.27	2.00	Skin	0.23	0.22
Stomach	2.19	2.14	Pulmonary trunk	0.05	0.11
Thyroid gland	1.61	1.50	Pulmonary veins	0.15	0.28
Visceral fat	1.25	0.54	Pulmonary arteries	0.15	0.28
Intestine	0.91	1.12	Other arteries	0.75	1.50
Trachea	0.68	0.71	Other veins	2.21	4.18
			Other tissues	0.64	0.60

5. Conclusion

In this work an unstructured mesh generation and numerical modeling technology for bioimpedance measurements is suggested. Possible applications include an analysis of sensitivity distributions for conventional (e.g., local or polysegmental) measurement schemes, as well as the development of new ones for specific purposes, optimization of electrode properties, their placement configurations and frequency spectra. Our approach enables mesh generation for high-resolution models with a significantly less number of mesh elements as compared to rectangular meshes thus reducing the computational costs.

Acknowledgements

This work was partially supported by the Russian Foundation for Basic Research (grants no. 11-01-00971, 10-01-91055), and the Federal Program “Academic and pedagogical staff of innovative Russia”.

References

[1] Caon M 2004 *Radiat. Environ. Biophys*. **42** 229-235
[2] Xu X G, Eckerman K F 2009 Handbook of anatomical models for radiation dosimetry (Boca Raton: CRC Press)
[3] Kauppinen P K, Hyttinen J A, Malmivuo J A 1998 *Ann. Biomed. Eng*. **26** 694-702
[4] Yang F, Patterson R 2010 in: 32nd Annual Int. Conf. of the IEEE EMBS. Buenos-Aires, Argentina, August 31- Sept. 4
[5] The Visible Human Project http://www.nlm.nih.gov/research/visible/visible_human.html
[6] Höhne K H, Pflesser B, Pommert A et al. 2001 *Meth. Inform. Med*. **40** 83-89
[7] Yushkevich P A, Piven J, Hazlett H C et al. 2006 *Neuroimage* **31** 1116-1128
[8] Wu Z, Sullivan J M 2003 *Int. J. Numer. Meth. Eng*. **58** 189-207
[9] Taubin G 1995 in: Proc. of the 22nd annual conference on computer graphics and interactive techniques (N.Y.: ACM) 351-358
[10] Frey P J, George P L 2000 Mesh generation: application to finite elements (Paris, Oxford: Hermes Science)
[11] Rineau L, Yvinec M 2007 *Comput. Geom. Theory Appl*. **38** 100-110
[12] 3D generator of anisotropic meshes http://sourceforge.net/projects/ani3d
[13] Kaporin I E 1998 *Numer. Linear Algebra Appl*. **5** 483-509
[14] Kubicek W G 1967 Pat. USA. №3.340.867 A61b.5/02 Sept.12
[15] Gabriel C, Peyman A, Grant E 2009 *Phys. Med. Biol*. **54** 4863-4878